Applied Microbiology and Biotechnology (2019) 103:6129–6139
https://doi.org/10.1007/s00253-019-09917-6

BIOTECHNOLOGICALLY RELEVANT ENZYMES AND PROTEINS

Enzymatic characterization of a thermostable phosphatase from *Thermomicrobium roseum* and its application for biosynthesis of fructose from maltodextrin

Dongdong Meng[1] · Ailing Liang[1,2] · Xinlei Wei[1] · Chun You[1]

Received: 1 February 2019 / Revised: 14 May 2019 / Accepted: 15 May 2019 / Published online: 6 June 2019

Abstract

Phosphatases, which catalyze the dephosphorylation of compounds containing phosphate groups, are important members of the haloacid dehalogenase (HAD)–like superfamily. Herein, a thermostable phosphatase encoded by an open reading frame of Trd_1070 from *Thermomicrobium roseum* was enzymologically characterized. This phosphatase showed promiscuous activity against more than ten sugar phosphates, with high specific activity toward ribose 5-phosphate, followed by ribulose 5-phosphate and fructose 6-phosphate. The half-life of Trd_1070 at 70 °C and pH 7.0 was about 14.2 h. Given that the catalytic efficiency of Trd_1070 on fructose 6-phosphate was 49-fold higher than that on glucose 6-phosphate, an in vitro synthetic biosystem containing alpha-glucan phosphorylase, phosphoglucomutase, phosphoglucose isomerase, and Trd_1070 was constructed for the production of fructose from maltodextrin by whole-cell catalysis, resulting in 21.6 g/L fructose with a ratio of fructose to glucose of approximately 2:1 from 50 g/L maltodextrin. This in vitro biosystem provides an alternative method to produce fructose with higher fructose content compared with the traditional production method using glucose isomerization. Further discovery and enzymologic characterization of phosphatases may promote further production of alternative monosaccharides through in vitro synthetic biosystems.

Keywords Phosphatase · Thermostable enzymes · HAD–like hydrolase · Substrate ambiguity · Fructose · In vitro synthetic enzymatic biosystems

Introduction

The ubiquitous haloacid dehalogenase (HAD)–like superfamily is a diverse superfamily comprised of enzymes that catalyze a wide range of reactions (Huang et al. 2015; Kuznetsova et al. 2015). To date, information of over 670,000 members of the HAD enzyme superfamily (IPR023214) have been deposited into the InterPro database (Mitchell et al. 2019). Phosphatases (CO–P cleavage) account for the vast majority of enzymes in the HAD superfamily (Burroughs et al. 2006; Zhang et al. 2004), followed by ATPases (PO–P cleavage) (Aravind et al. 1998; Collet et al. 1998b), phosphonatases (C–P cleavage) (Morais et al. 2000), dehalogenases (C–Cl cleavage) (Motosugi et al. 1982), and sugar phosphomutases (CO–P cleavage/formation) (Collet et al. 1998a). Numerous types of HAD phosphatases are present in cells of both prokaryotes and eukaryotes. For example, at least 23 members of HAD phosphatases have been discovered in *Escherichia coli* and at least 19 members have been found in yeast (Kuznetsova et al. 2015; Kuznetsova et al. 2006). In brief, HAD phosphatases play different cellular roles on various aspects, including the maintenance of metabolic pools, the regulation of primary and secondary metabolism, cell housekeeping, and the uptake of nutrients (Allen and Dunaway-Mariano 2004; Kuznetsova et al. 2006; Rangarajan et al. 2006; Rinaldo-Matthis et al. 2002; Wang et al. 2001). For example, phosphoserine phosphatase participates in the biosynthesis of L-serine by catalyzing the dephosphorylation of

Electronic supplementary material The online version of this article (https://doi.org/10.1007/s00253-019-09917-6) contains supplementary material, which is available to authorized users.

✉ Chun You
you_c@tib.cas.cn

[1] Tianjin Institute of Industrial Biotechnology, Chinese Academy of Sciences, 32 West 7th Avenue, Tianjin Airport Economic Area, Tianjin 300308, People's Republic of China

[2] School of Biotechnology, Tianjin University of Science and Technology, Tianjin 300457, People's Republic of China

phospho-L-serine (Wang et al. 2001). Deoxyribonucleotidase, a ubiquitous enzyme in mammalian cells, dephosphorylates nucleoside monophosphates and functions to balance the nucleoside pools (Rinaldo-Matthis et al. 2002). 2-Deoxyglucose-6-phosphatase helps to reduce the intracellular level of 2-deoxyglucose-6-phosphate, which is a toxic analogue of glucose 6-phosphate (G6P) and represses cell growth at high concentrations (Kuznetsova et al. 2006).

The HAD phosphatases have a highly conserved α/β "core" domain that contains the phosphoryl transfer site (Lu et al. 2008) and a "cap" domain that acts as a dynamic lid over the core domain of the active site to provide the substrate specificity determinants (Lahiri et al. 2004). In a previous study, Huang et al. have examined the activity profile of more than 200 HAD phosphatases by screening a customized library of 167 compounds. Their result has demonstrated that 75% of HAD phosphatases can utilize greater than five substrates (Huang et al. 2015). For instance, more than half of the characterized phosphatases from *Saccharomyces cerevisiae* and *E. coli* show high promiscuous activity against multiple phosphorylated metabolites (Kuznetsova et al. 2015; Kuznetsova et al. 2006). Thus, HAD phosphatases exhibit an extremely high level of substrate ambiguity, which may serve to avoid the accumulation of phosphorylated metabolites, to sufficiently metabolize large pools of similar substrates, and to facilitate the evolution of new metabolic function in response to a change in the substrate pool caused by environmental challenges (Huang et al. 2015).

The numerous HAD phosphatases provide us with a large amount of versatile enzyme candidates that can be used to produce a variety of biochemicals via dephosphorylation of phosphate group–containing metabolites. For example, inositol monophosphatase was used to produce inositol via an in vitro enzymatic biosystem (You et al. 2017), the HAD-like phosphatase YqaB was introduced into *S. cerevisiae* to produce N-acetylglucosamine (Lee and Oh 2016), sorbitol-6-phosphate phosphatase SorPP was used for the biosynthesis of sorbitol (Zhou et al. 2003), and a possible fructose-6-phosphatase was proposed for the biosynthesis of fructose (Moradian and Benner 1992). Nevertheless, substrate specificity has not been well characterized for a large number of phosphatases, which prohibited the use of these enzymes in the synthesis of value-added biochemicals. Accurate information on substrate specificity is therefore key prerequisite for the successful application of HAD phosphatases.

In vitro synthetic enzymatic biosystems are regarded as the next-generation biomanufacturing platform featured by their high product yield, fast reaction rate, great engineering flexibility, and easy scale-up (You and Zhang 2017). Generally, thermostable enzymes from thermophilic microorganisms are recommended for in vitro biosystems due to their operational stability and low risk of contamination (You and Zhang 2017). Recombinant thermophilic enzymes overexpressed in mesophilic hosts (such as *E. coli*) can be purified via a simple heat precipitation process, which lowers the cost of enzyme preparation (You et al. 2017). In addition, high operating temperature decreases viscosity of the aqueous reaction solutions and consequently enhances the mass transfer (You et al. 2017). Whole-cell biocatalysts utilizing recombinant thermophilic enzymes are considered to be a promising alternative to purified enzymes in industrial processes due to several advantages. These advantages include (i) higher stability compared purified enzymes; (ii) reduced purification requirements because insoluble cell catalysts can be collected through centrifugation after a heat treatment step; (iii) independence of exogenous cofactors and avoidance of possible toxic constraints; and (iv) more stability of the enzymes upon immobilization, which is a process that can achieve robust reusability (Dong et al. 2017; Kim et al. 2014; Ninh et al. 2013).

In this study, we performed the functional assignment of HAD phosphatase Trd_1070 (GeneBank accession no. ACM05684) from *Thermomicrobium roseum* DSM 5159, which was previously uncharacterized. Sequence analysis and substrate specificity assay were carried out to clarify the substrate spectrum of Trd_1070. Then, enzymatic characterization of Trd_1070 was performed to deep understand its basic properties. On the basis of the characterized enzymatic properties, *E. coli* whole-cell biocatalysts containing overexpressed Trd_1070 as well as three other thermostable enzymes, alpha-glucan phosphorylase (αGP), phosphoglucomutase (PGM), and phosphoglucose isomerase (PGI), were mixed and applied to the biosynthesis of fructose from maltodextrin via a reported in vitro enzymatic biosystem (Moradian and Benner 1992).

Materials and Methods

Bacterial strains and culture conditions

E. coli TOP10 and BL21 (DE3) were used for plasmid propagation and protein expression, respectively. The *E. coli* strains were grown in Luria−Bertani (LB) medium at 37 °C with 100 μg/mL ampicillin (Solarbio, China) when required. Unless otherwise indicated, other analytical reagents were purchased from Sigma-Aldrich (USA).

Sequence analysis of Trd_1070

According to the protein sequence, function prediction and homology analysis of *T. roseum* Trd_1070 were performed using the NCBI (National Center for Biotechnology Information, USA) database. Sequence alignment of Trd_1070 and its homologous proteins was performed by using ClustalW (http://clustalw.ddbj.nig.ac.jp/), and the

phylogenetic tree was constructed by MEGA 6.0 software using a neighbor-joining method (Tamura et al. 2013).

Cloning, expression, and purification of Trd_1070

The gene encoding Trd_1070 from *T. roseum* was synthesized by General Biosystems (Anhui) Co., Ltd. (Anhui, China) with codon optimization, yielding plasmid pET15b-Trd_1070. *E. coli* BL21 (DE3) harboring the recombinant expression vector was cultured in LB medium at 37 °C and 220 rpm until the optical density at 600 nm ($OD_{600\ nm}$) reached 0.6–0.8. 0.1 mM isopropyl-β-D-thiogalactopyranoside (IPTG) was then added into the shake flask, and the bacterial culture was transferred to 16 °C for another 16 h of cultivation. Cells were harvested by centrifugation at 4 °C and were resuspended in lysis buffer (50 mM HEPES, 50 mM NaCl, pH 7.5). After ultrasonication on ice, cell debris was removed by centrifugation at 12,000×*g* for 20 min at 4 °C. The crude enzyme was loaded onto a nickel-nitrilotriacetic acid (Ni-NTA) affinity column to purify the His-tagged Trd_1070. The targeting eluent was buffer exchanged to 50 mM HEPES buffer (pH 7.0) by ultrafiltration (10-kDa cutoff membrane; Millipore, Billerica, USA) at 4 °C. The homogeneity of the proteins was checked using 12% SDS-PAGE. Protein concentrations were determined by the Bradford method with bovine serum albumin as the standard.

Measurement of enzyme activity

The substrate specificity assays were performed at 80 °C for 10 min in HEPES buffer (pH 7.0) containing 5 mM $MgCl_2$ and an appropriate amount of Trd_1070. Different sugar phosphates, including ribose 5-phosphate (R5P), ribulose 5-phosphate (Ru5P), fructose 6-phosphate (F6P), xylulose 5-phosphate (Xu5P), deoxyribose 5-phosphate (DR5P), fructose 1,6-diphosphate (F16P), glyceraldehyde 3-phosphate (G3P), dihydroxyacetone phosphate (DHAP), tagatose 6-phosphate (T6P), glucose 6-phosphate (G6P), allulose 6-phosphate (A6P), glucosamine 6-phosphate (GlcN6P), glucose 1-phosphate (G1P), mannose 6-phosphate (M6P), and inositol 1-phosphate (I1P), were tested one at a time at a final concentration of 10 mM. The reaction was stopped by $HClO_4$ and neutralized by KOH (You and Zhang 2013). The released inorganic phosphate was measured by the mild pH phosphate assay (Saheki et al. 1985). One unit (U) of enzyme activity was defined as the amount of enzyme that released 1 μmol of phosphate per minute. The activity of Trd_1070 against the general phosphatase substrate *p*-nitrophenyl phosphate (*p*NPP) at a final substrate concentration of 1 mM was performed in HEPES buffer (pH 7.0) containing 5 mM $MgCl_2$ at 80 °C. The reaction was halted by adding sodium carbonate to a final concentration of 0.75 M. The absorbance of released *p*-nitrophenol was detected at 405 nm. One unit of enzyme activity was defined as the amount of enzyme that liberated 1 μmol of *p*-nitrophenol per minute. Unless otherwise stated, each measurement was conducted in triplicate, and error bars are reported as standard deviations.

Effects of temperature and pH on Trd_1070 activity

The effects of temperature and pH on Trd_1070 activity and stability were evaluated using *p*NPP as substrate. For determining the enzymatic optimal temperature, activities of Trd_1070 were measured from 30 to 95 °C in 100 mM HEPES buffer (pH 7.0) containing 5 mM $MgCl_2$. One hundred millimolars of Bis-Tris buffer (pH 6.0–7.0), 100 mM HEPES buffer (pH 7.0–8.0), and 100 mM Tris-HCl buffer (pH 8.0–9.0) were used for optimal pH determination at 80 °C. The thermostability of Trd_1070 was determined at 60, 70, and 80 °C in 100 mM HEPES buffer (pH 7.0). Aliquots of samples were taken at different time points, and the residual activity was determined immediately by using *p*NPP as substrate.

Effects of cations on Trd_1070 activity

To examine the effects of cations on the activity of Trd_1070, NH_4^+, Ca^{2+}, Mg^{2+}, Fe^{2+}, Fe^{3+}, Co^{2+}, Ni^{2+}, Cu^{2+}, Mn^{2+}, and Zn^{2+} were added to a final concentration of 1 mM each at a time. The effect of Mg^{2+} concentration on the enzymatic activity of Trd_1070 was also tested. After pre-incubation in HEPES buffer (pH 7.0) with the cations for 1 h at 4 °C, the activity was determined using *p*NPP as substrate at 80 °C. The Trd_1070 activity in the absence of the cations listed above was considered 100%.

Determination of kinetic parameters of the purified enzyme

The Michaelis–Menten kinetic parameters of purified Trd_1070 were determined at pH 7.0 and 70 °C using several substrates, including *p*NPP, G1P, G6P, and F6P. 0.246 mg/L of Trd_1070 was incubated with *p*NPP at various concentrations from 0.01 to 1 mM for 5 min. 0.516 g/L of Trd_1070 was incubated with G1P at various concentrations from 0.5 to 20 mM for 60 min. 0.516 g/L of Trd_1070 was incubated with G6P at various concentrations from 0.5 to 20 mM for 30 min. 0.086 g/L of Trd_1070 was incubated with F6P at various concentrations from 0.2 to 10 mM for 3 min. The amounts of the catalytic product, *p*-nitrophenol or phosphate, were detected and were plotted against substrate concentrations to calculate the initial reaction rates. Kinetic constants (the Michaelis constant K_m and the turnover number k_{cat}) were estimated using the Michaelis–Menten equation with GraphPad Prism 5.01 software (San Diego, CA, USA) by employing nonlinear regression.

Application of Trd_1070 to the production of fructose from maltodextrin

Plasmids pET20b-TmαGP, pET20b-TkPGM, and pET28a-TtcPGI were used for the preparation of corresponding recombinant proteins, namely alpha-glucan phosphorylase (αGP) from *Thermotoga maritima* DSM 3109, phosphoglucomutase (PGM) from *Thermococcus kodakarensis* ATCC BAA-918, and phosphoglucose isomerase (PGI) from *Thermus thermophilus* DSM 46338, respectively, by methods as described elsewhere (Wang et al. 2017; You et al. 2017). pET15b-Trd_1070 was used for the expression of the phosphatase Trd_1070. pET20b-StIA was used to express *Sulfolobus tokodaii* DSM 16993 isoamylase (IA), which debranched maltodextrin by hydrolyzing α-1,6-glucosidic linkages (Zhou et al. 2016). Each recombinant *E. coli* strain was cultivated in a 5-L fermenter (T&J Bioengineering Co., Ltd., Shanghai, China) at 37 °C using high-cell-density media with a slightly modified formulation that the citric acid and thiamine were replaced with 10 g/L yeast extract (Riesenberg et al. 1991). In the fed-batch phase, the specific growth rate was controlled at 0.10 per hour, the pH value was controlled at 6.7–7.2, and the dissolved oxygen level was controlled to be more than 20%. Protein expression was induced by adding 100 mg lactose/g dry cell/h at 16 °C. The cells were then harvested by centrifugation (5,000×*g*, 20 min, 4 °C), washed twice, and stored at − 20 °C. For the preparation of the whole-cell catalyst, the cells were resuspended in HEPES buffer (50 mM, pH 7.0) and subsequently heated at 70 °C for 20 min.

The pretreatment of maltodextrin was conducted by mixing 1 U/mL of IA with 100 g/L maltodextrin (DE 4-7) in 5 mM acetate buffer (pH 5.5) containing 0.5 mM $MgCl_2$. After incubation at 80 °C for 3 h, the IA-treated maltodextrin was obtained. One-pot biosynthesis of fructose was conducted in 100 mM HEPES (pH 7.0) containing 10 g/L IA-treated maltodextrin, 20 mM phosphate, and 5 mM $MgCl_2$ at 70 °C under anaerobic condition. In the proof-of-concept assay, the heat-treated cells expressing αGP, PGM, PGI, and Trd_1070 were added under loading amounts of 0.10 U/mL for each. After process optimization, the reaction mixture containing 0.15 U/mL αGP-containing cells, 0.15 U/mL PGM-containing cells, 0.60 U/mL PGI-containing cells, and 0.10 U/mL Trd_1070-containing cells was constructed to produce fructose from 10 g/L IA-treated maltodextrin. For a high substrate concentration of 50 g/L IA-treated maltodextrin, the reaction was performed at 70 °C under anaerobic condition in 100 mM HEPES buffer (pH 7.0) containing 10 mM $MgCl_2$, 50 mM phosphate, 0.30 U/mL αGP-containing cells, 0.30 U/mL PGM-containing cells, 1.2 U/mL PGI-containing cells, and 0.20 U/mL Trd_1070-containing cells. The reaction was carried out with a stirring speed of 120 rpm. Samples were collected at different time points. Fructose in the supernatant were determined by an HPLC apparatus equipped with a Bio-Rad HPX-87H column with 5 mM H_2SO_4 as a mobile phase and a refractive index detector. The concentration of glucose was determined by a glucose oxidase/peroxidase assay kit. G1P was determined using a coupled spectrophotometric assay by a self-made G1P assay kit (100 mM HEPES buffer at pH 7.5, 1 U/mL of glucose 6-phosphate dehydrogenase (G6PDH, EC 1.1.1.49), 1 U/mL of PGM, 0.15 mM NAD^+, 5 mM $MgCl_2$). The generation of NADH was monitored at 340 nm. G6P was measured by a self-made G6P assay kit (100 mM HEPES buffer at pH 7.0, 1 U/mL of G6PDH, 0.15 mM NAD^+, 5 mM $MgCl_2$) by monitoring the absorbance increase at 340 nm. F6P was determined by the G6P assay kit supplemented with 1 U/mL PGI. The concentration of maltodextrin was determined by the amylose/amylopectin assay kit (Megazyme, Wicklow, Ireland). Unless otherwise stated, each measurement was conducted in triplicate, and error bars are reported as standard deviations.

Sequence submission

The nucleotide sequence of codon-optimized full-length Trd_1070 gene was deposited in the GenBank database under the accession number of MK496545.

Results

Sequence analysis, expression, and purification of recombinant Trd_1070

In the genome of *T. roseum* DSM 5159, the open reading frame (ORF) of Trd_1070 gene encoded a 294 amino acid protein (GenBank accession no. ACM05684.1), which was annotated as N-acetylglucosamine-6-phoshatase or *p*-nitrophenyl phosphatase. Trd_1070 shared the highest sequence identity of 78% to a putative acid sugar phosphatase from bacterium HR28 (GenBank accession no. GBD20727.1), which was a previously uncharacterized enzyme. Among the characterized enzymes, the one with the highest sequence identity to Trd_1070 was the thermostable *p*-nitrophenyl phosphatase (NPPase) from *Geobacillus stearothermophilus* (GenBank accession no. AAM29189.1; with 37% sequence identity to Trd_1070) (Shen et al. 2014), followed by the glycerol 3-phosphate phosphatase from *Mycobacterium tuberculosis* (GenBank accession no. CCP44457.1; with 29% sequence identity to Trd_1070) (Larrouy-Maumus et al. 2013) and the ribonucleotide monophosphatase from *E. coli* (GenBank accession no. CAA32355.1; with 27% sequence identity to Trd_1070) (Tremblay et al. 2006). Sequence alignment and phylogenetic analysis indicated that Trd_1070 clustered with a wide range of phosphatases from HAD–like hydrolase superfamily (Fig. 1a). However, the enzymatic

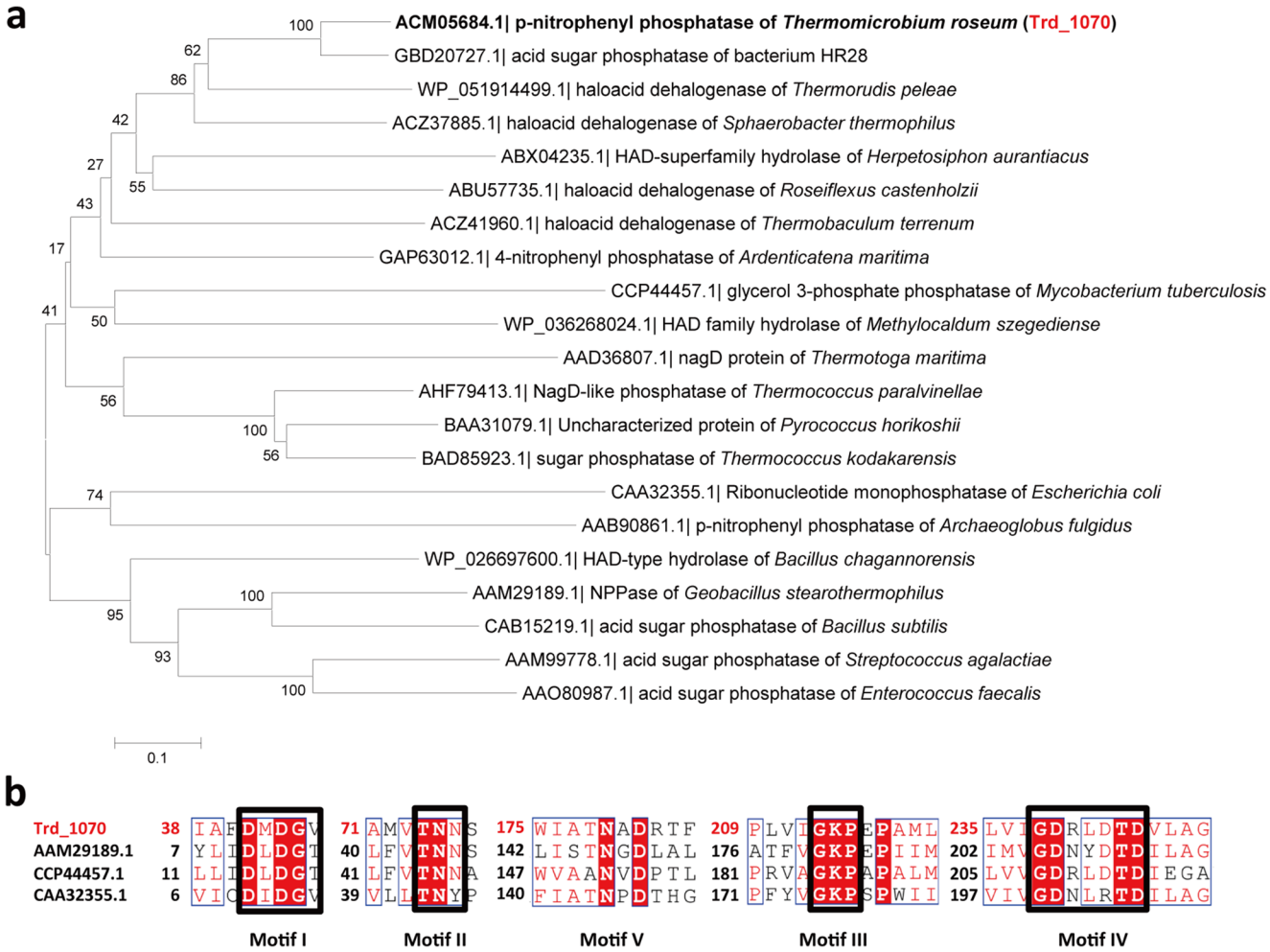

Fig. 1 Bioinformatics analysis of Trd_1070. **a** Neighbor-joining phylogenetic tree. Phylogenetic analysis was carried out using MEGA 6.0 software. **b** Multiple sequence alignments of Trd_1070 and three characterized homologous HAD–like phosphatases on conservative motifs I–V. AAM29189.1, *p*-nitrophenyl phosphatase (NPPase) from *G. stearothermophilus*; CCP44457.1, glycerol 3-phosphate phosphatase from *M. tuberculosis*; CAA32355.1, ribonucleotide monophosphatase from *E. coli*

properties, especially substrate specificity, of most of these enzymes had not been determined so far. To look for more evidence that Trd_1070 belongs to the HAD superfamily, we also examined the sequence motifs shared by Trd_1070 and the three characterized HAD–like phosphatases mentioned above. HAD enzymes possess a typical structure consisting of four loops (corresponding to four sequence motifs) and a mobile cap domain (Fig. 1b) (Allen and Dunaway-Mariano 2004). Motif I (DXDX(T/V)) is the catalytic center and is associated with Mg^{2+} cofactor binding (Collet et al. 1998a; Guo et al. 2014). Motif II (S/TXX) is responsible for the formation of hydrogen bond with oxygen in phosphate radical (Guo et al. 2014). Motifs III (XKX) and IV ((G/S)(D/S)X2-6(D/N)) both play a role in the orientation of the nucleophile and the coordination of Mg^{2+} (Collet et al. 1998a; Guo et al. 2014). The cap domain (motif V) determines substrate specificity (Guo et al. 2014; Lahiri et al. 2004). On the basis of the sequence and structure information of the three characterized phosphatases, the conservative motifs I–V of Trd_1070 was predicted (Fig. 1b), suggesting that Trd_1070 was a putative HAD–like phosphatase.

The codon-optimized full-length Trd_1070 gene was synthesized and was successfully expressed in *E. coli* BL21 (DE3) with a C-terminal His-tag. The recombinant protein was purified by Ni-NTA column. According to SDS-PAGE analysis, Trd_1070 was purified to homogeneity and showed a single band with a molecular weight of 32 kDa, which was consistent with the predicted value based on amino acid sequence (Fig. 2). Approximately 3.44 mg of Trd_1070 was purified from 200 mL of the cell culture with a purification yield of 36.1%.

Substrate specificity of Trd_1070

Substrate specificity of recombinant Trd_1070 toward a range of sugar phosphates and *p*NPP was analyzed. Trd_1070 could decompose *p*NPP with a specific activity of 98.6 U/mg at 80 °C, yielding phosphate, and a yellow product, *p*-nitrophenol.

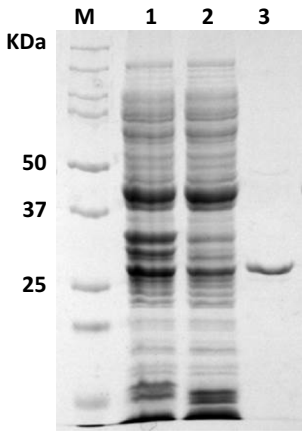

Fig. 2 SDS-PAGE analysis of Trd_1070 purified from recombinant *E. coli* BL21 (DE3). Lane 1, cell lysate containing Trd_1070; lane 2, supernatant of the soluble cell lysate containing Trd_1070; lane 3, purified Trd_1070 by Ni-NTA column

This result indicated that Trd_1070 was able to process phosphorylated substrates. At 80 °C and pH 7.0, the specific activity of purified Trd_1070 was 0.99 U/mg against R5P, 0.66 U/mg against Ru5P, 0.59 U/mg against F6P, 0.29 U/mg against Xu5P, 0.26 U/mg against DR5P, 0.22 U/mg against F16P, and only 0.01–0.1 U/mg against other nine phosphorylated substrates (Fig. 3). This result suggested that Trd_1070 was highly promiscuous. Trd_1070 demonstrated the highest specific activity toward R5P, and a comparable activity toward other pentose phosphates such as Ru5P and Xu5P. Because Ru5P, Xu5P, and R5P might simultaneously exist as intermediates in the process of pentose production, Trd_1070 would dephosphorylate all these intermediates to result in a mixture of ribose, ribulose, and xylulose in similar proportions, which would in turn lead to low yield and high separation cost of the desired product. The similar activities of Trd_1070 on the dephosphorization of different pentose phosphates suggested that Trd_1070 was unsuitable to produce pentose. By contrast, the activity of Trd_1070 for F6P was 6-fold higher than that for the other hexose phosphates such as G6P and G1P (Fig. 3). This property of Trd_1070 made it a potential phosphatase to produce fructose.

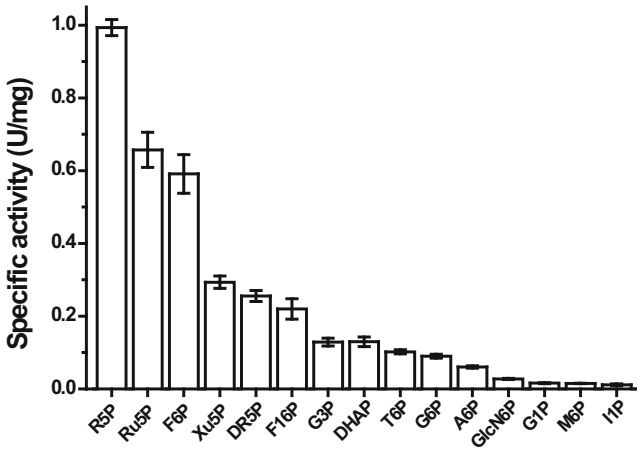

Fig. 3 Substrate specificity of Trd_1070. The sugar phosphates used were ribose 5-phosphate (R5P), ribulose 5-phosphate (Ru5P), fructose 6-phosphate (F6P), xylulose 5-phosphate (Xu5P), deoxyribose 5-phosphate (DR5P), fructose 1,6-diphosphate (F16P), glyceraldehyde 3-phosphate (G3P), dihydroxyacetone phosphate (DHAP), tagatose 6-phosphate (T6P), glucose 6-phosphate (G6P), allulose 6-phosphate (A6P), glucosamine 6-phosphate (GlcN6P), glucose 1-phosphate (G1P), mannose 6-phosphate (M6P), and inositol 1-phosphate (I1P)

Effects of temperature, pH, and cations on the activity of Trd_1070

Using 1 mM of *p*NPP as substrate, the optimal temperature and pH of Trd_1070 were determined to be 80 °C and 7.0, respectively (Fig. S1a and S1b). Thermostability of Trd_1070 in 100 mM HEPES buffer (pH 7.0) strongly depended on temperature. At 4.3 mg/L, the half-life of Trd_1070 was 3.7 h, 0.6 h, and 0.09 h at 60, 70, and 80 °C, respectively (Fig. S1c). The effect of mass concentration on the thermostability was determined at 0.86 g/L Trd_1070. In this case, the half-life time of thermo-inactivation was extended to about 71.2 h, 14.2 h, and 0.2 h at 60, 70, and 80 °C, respectively (Fig. S1d). Therefore, Trd_1070 was a phosphatase with excellent thermostability, and the stability was temperature- and mass concentration-dependent (Table 1).

Trd_1070 was slightly activated by Fe^{3+} and Ni^{2+} with a relative activity of 140% and 141%, respectively. The enzyme was significantly activated by 1 mM Mg^{2+}, exhibiting a 4.6-fold increase of specific activity (Fig. 4a). In addition, the activity of Trd_1070 increased as the Mg^{2+} concentration increased to 5 mM (Fig. 4b). The results suggested that Trd_1070 was a Mg^{2+}-dependent phosphatase.

Enzymatic kinetics analysis of Trd_1070

The kinetic parameters of Trd_1070 were measured against *p*NPP and hexose phosphates in 100 mM HEPES buffer (pH 7.0) containing 5 mM $MgCl_2$ at 70 °C (Table 2). The K_m and k_{cat} values of Trd_1070 for *p*NPP were 0.09 mM and 5321.1 min^{-1}, respectively, which led to a high catalytic efficiency (k_{cat}/K_m) of the enzyme (59123.3 mM^{-1} min^{-1}). The catalytic efficiency values of Trd_1070 against sugar phosphates were relative lower than that of Trd_1070 against *p*NPP. The K_m value of Trd_1070 for F6P was comparable to those for G1P and G6P. However, the k_{cat}/K_m value of Trd_1070 for F6P was one and two orders higher than those for G6P and G1P, respectively (Table 2). These results indicated that Trd_1070 had much higher activity against F6P compared with G1P and G6P, and was consistent with the results of substrate specificity experiment. On the basis of the above results of enzymatic characterization, we speculated that Trd_1070 could be applied to a reported in vitro synthetic enzymatic biosystem

Table 1 Enzymatic characteristics of Trd_1070

Enzyme	Optimal temp (°C)	Optimal pH	Half-life of Trd_1070	
			Incubation concentration of Trd_1070 under 4.3 mg/L	Incubation concentration of Trd_1070 under 0.86 g/L
Trd_1070	80	7.0	3.7 h under 60 °C	71.2 h under 60 °C
			0.6 h under 70 °C	14.2 h under 70 °C
			0.09 h under 80 °C	0.2 h under 80 °C

containing alpha-glucan phosphorylase (αGP, phosphoglucomutase (PGM), phosphoglucose isomerase (PGI), and fructose-6-phosphatase for the production of fructose from maltodextrin (Moradian and Benner 1992).

Fructose biosynthesis by a Trd_1070-containing whole-cell biosystem

On the basis of the enzymatic properties of Trd_1070, an in vitro enzymatic biosystem containing Trd_1070 was constructed to produce fructose from maltodextrin (Fig. 5a). The reaction pathway consisted of four sequential steps: (1) maltodextrin was phosphorolyzed by αGP in the presence of inorganic phosphate, yielding G1P; (2) G1P was converted to G6P by PGM; (3) G6P was isomerized to F6P by PGI; (4) F6P was dephosphorylated into fructose and phosphate by Trd_1070. Inorganic phosphate could be recycled between reactions 1 and 4 in one vessel. The standard Gibbs energy changes (ΔG′°) of reactions 1 to 4 were calculated to be + 2.8, − 7.4, + 2.5, and − 11.7 kJ/mol at pH 7.0 and ionic strength of 0.1 M (http://equilibrator.weizmann.ac.il/), respectively (Table 3). Although reactions of steps 1 and 3 were thermodynamically unfavorable, their downstream exergonic reactions, especially the reaction catalyzed by Trd_1070, helped to push the overall reaction toward the desired direction.

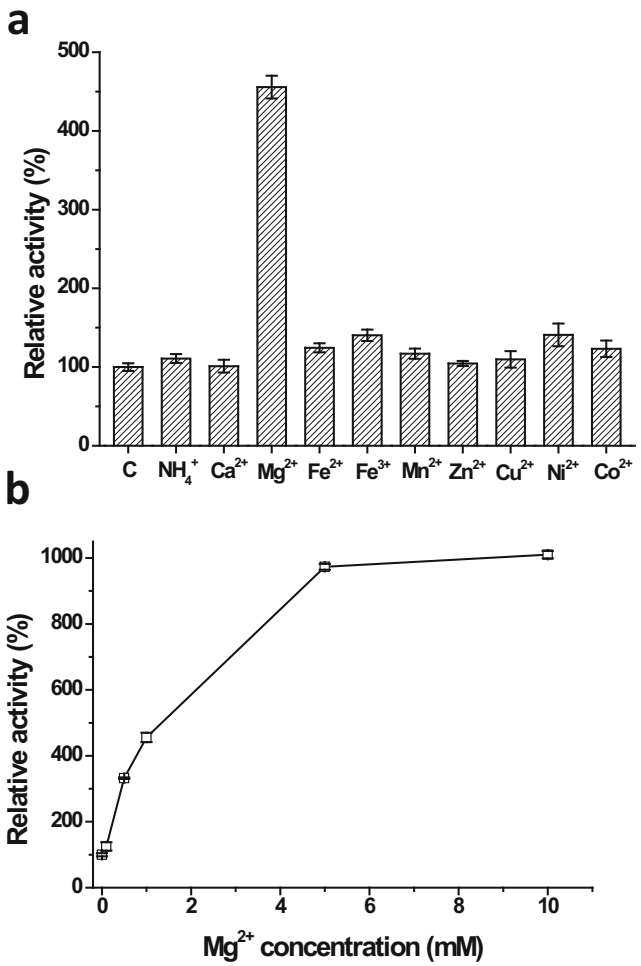

Fig. 4 Effects of cations on the enzymatic activity of Trd_1070. **a** The relative activity of Trd_1070 at 1 mM cations. **b** The effect of Mg^{2+} concentration on the activity of Trd_1070. The Trd_1070 activity in the absence of any cations was considered 100%

Whole-cell biocatalyst is a useful tool to produce biochemicals due to its high stability, reduced purification requirement, and low preparation cost (Dong et al. 2017; Kim et al. 2014). Therefore, whole-cell biocatalysts of four BL21 (DE3) strains containing *T. maritima* αGP (gene locus TM1168), *T. kodakarensis* PGM (gene locus TK1108), *T. thermophilus* PGI (gene locus TTHA0277), and *T. roseum* Trd_1070, respectively, were mixed and applied to produce fructose from maltodextrin. The specific activities of 1 $OD_{600\ nm}$ of whole-cell biocatalysts αGP, PGM, PGI, and Trd_1070 were 37.5 mU/mL, 81.0 mU/mL, 300.0 mU/mL, and 1.4 mU/mL, respectively. At the beginning, 10 g/L maltodextrin (58.1 mM glucose equivalent) was used for the proof-of-concept experiment of this in vitro enzymatic biosystem when the loading amounts of all four whole-cell biocatalysts are 0.10 U/mL. The HPLC spectra showed that the whole-cell biosystem can convert maltodextrin into fructose successfully, accompanied with a high concentration of by-product of glucose which was

Table 2 The kinetic characteristics of Trd_1070 against phosphorylated substrates in 100 mM HEPES (pH 7.0) containing 5 mM $MgCl_2$ at 70 °C

Substrate	k_{cat} (min^{-1})	K_m (mM)	k_{cat}/K_m ($mM^{-1}\ min^{-1}$)
pNPP	5321.1	0.09	59123.3
G1P	0.2	2.4	0.1
G6P	4.8	7.5	0.6
F6P	74.0	2.5	29.6

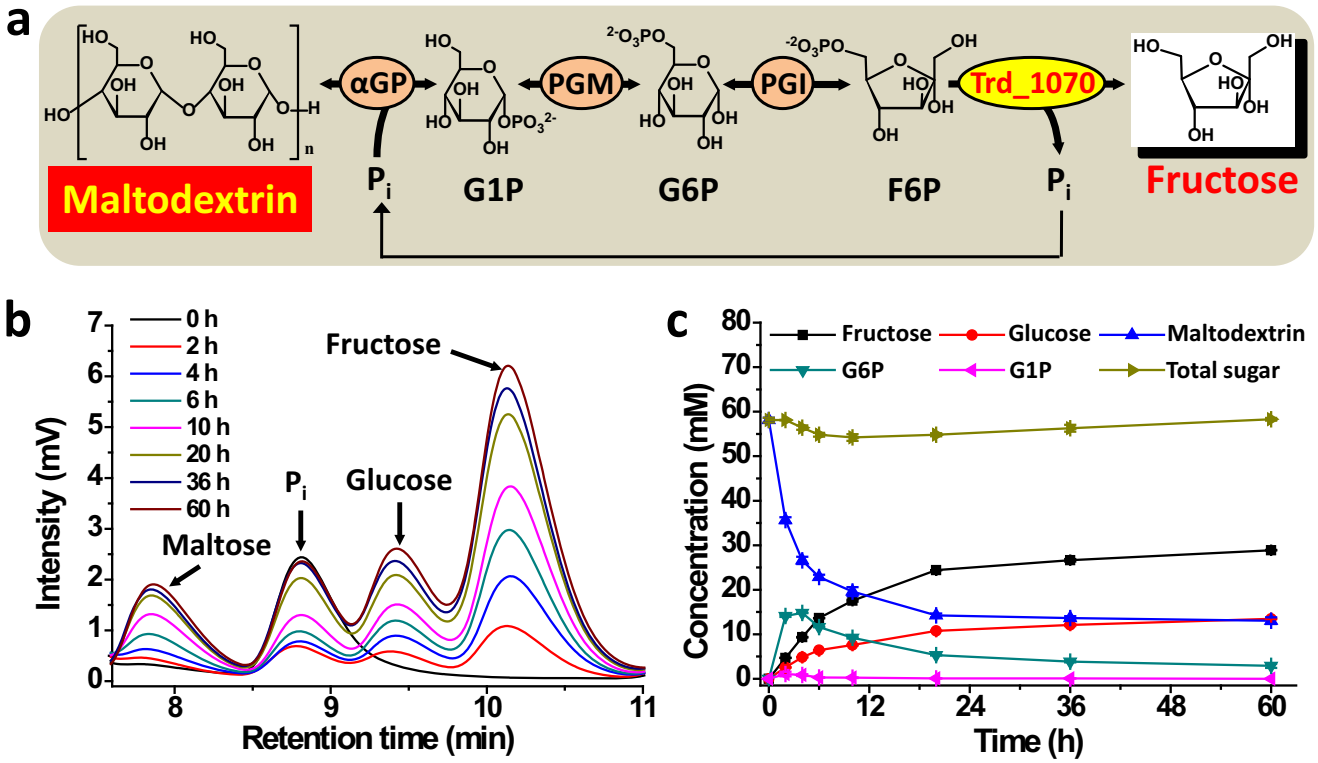

Fig. 5 Biosynthesis of fructose from 10 g/L maltodextrin via an in vitro synthetic enzymatic biosystem. **a** Scheme of the ATP- and cofactor-free in vitro enzymatic biosystem for the synthesis of fructose from maltodextrin. The enzymes were alpha-glucan phosphorylase (αGP), phosphoglucomutase (PGM), phosphoglucose isomerase (PGI), and phosphatase (Trd_1070). The intermediates were glucose 1-phosphate (G1P), glucose 6-phosphate (G6P), and fructose 6-phosphate (F6P). **b** HPLC profiles of reaction systems at different time points. **c** Concentration profiles of substrates and products. The reaction was performed at 70 °C under the condition of 10 g/L IA-treated maltodextrin (58.1 mM glucose equivalent), 100 mM HEPES buffer (pH 7.0), 10 mM $MgCl_2$, 20 mM phosphate, 0.15 U/mL αGP-containing cells, 0.15 U/mL PGM-containing cells, 0.60 U/mL PGI-containing cells, and 0.10 U/mL Trd_1070-containing cells

caused by the futile dephosphorylation of G6P by Trd_1070 (Fig. S2a). The concentration values of fructose and glucose were 12.5 mM (2.3 g/L) and 7.8 mM (1.4 g/L) at hour 20, respectively (Fig. S2b).

The reaction conditions of this biosystem were optimized to improve the product yield of fructose. The reaction temperature was first determined. The reactions were performed at 60, 70, and 80 °C (Fig. S3a). Although a high titer of fructose (14.6 mM) was obtained under 80 °C at 20 h, the biosystem can produce a comparable concentration of fructose (12.9 mM) with a mole ratio of fructose to glucose (F/G) of 1.59 under 70 °C at 20 h. In addition, the optimal temperature of Trd_1070 is 80 °C, and the reaction temperature of this in vitro enzymatic biosystem was set at 70 °C to avoid thermal inactivation of Trd_1070. Then the reactions were performed from pH 6.0 to 8.0 at 70 °C. This whole-cell biosystem can produce 12.0 mM, 12.3 mM, and 11.2 mM fructose in pH 6.5, 7.0, and 7.5, respectively (Fig. S3b). Thus, the pH value of 7.0 was selected as the optimal pH. The ratio of four different whole-cell biocatalysts was optimized under 70 °C and pH 7.0 according to the fructose concentrations

Table 3 The information of enzymes used in this in vitro synthetic enzymatic biosystem

Enzyme	EC no.	Source	Gene locus	$\Delta G'^{oa}$	K_{eq} [a]
Alpha-glucan phosphorylase (αGP)	2.4.1.1	*T. maritima*	TM1168	2.8	0.3
Phosphoglucomutase (PGM)	5.4.2.2	*T. kodakarensis*	TK1108	− 7.4	20.0
Phosphoglucose isomerase (PGI)	5.3.1.9	*T. thermophilus*	TTHA0277	2.5	0.4
Fructose-6-phosphatase (Trd_1070)	–	*T. roseum*	Trd_1070	− 11.7	115.0

[a] The standard Gibbs energy changes ($\Delta G'^{o}$) and the theoretical equilibrium constants (K_{eq}) were calculated by using the calculator at http://equilibrator.weizmann.ac.il/ at pH 7.0 and an ionic strength = 0.1 M

and F/G values (Fig. S4). The optimal ratio of heat-treated whole-cell biocatalysts αGP, PGM, PGI, and Trd_1070 was determined as 3:3:12:2 at the loading amounts of 0.15 U/mL (4 $OD_{600\ nm}$), 0.15 U/mL (1.85 $OD_{600\ nm}$), 0.60 U/mL (2 $OD_{600\ nm}$), and 0.10 U/mL (71.4 $OD_{600\ nm}$) for converting 10 g/L maltodextrin, respectively.

Then, we performed fructose production experiments under the optimal conditions. HPLC was used to quantify the concentrations of fructose and glucose (Fig. 5b). The concentration of maltodextrin rapidly decreased before hour 10 and the residual maltodextrin was 13.1 mM in glucose equivalent at hour 60. Meanwhile, the concentration of fructose gradually increased to 5.2 g/L (28.9 mM) at hour 60 with a fructose yield of 49.7% (Fig. 5c), and the by-product glucose was maintained at a concentration of 2.4 g/L (13.5 mM) at hour 60. The main intermediate of this biosystem was G6P, which reached a highest concentration of 14.8 mM at hour 4 and gradually decreased to 2.9 mM at hour 60. The concentration of total sugar was maintained at a relatively constant level (Fig. 5c).

Subsequently, this biosystem was analyzed using 50 g/L IA-treated maltodextrin (277.5 mM glucose equivalent) as substrate to investigate its potential for industrial applications. Generally, the enzyme amounts on 50 g/L maltodextrin should be 5 times of those on 10 g/L maltodextrin. However, 357 $OD_{600\ nm}$ of Trd_1070, which was 5 times of that on 10 g/L maltodextrin, was too much to be added into the reaction system containing 50 g/L maltodextrin. Thus, 2 times of enzyme loadings on 10 g/L maltodextrin were chosen to produce fructose from 50 g/L maltodextrin, while the ratio of the four enzymes remained the same. Less enzyme loadings should only affect the reaction time. As shown in Fig. 6, at hour 96, the concentrations of fructose and glucose were 21.6 g/L (120.2 mM) and 9.8 g/L (54.5 mM), respectively.

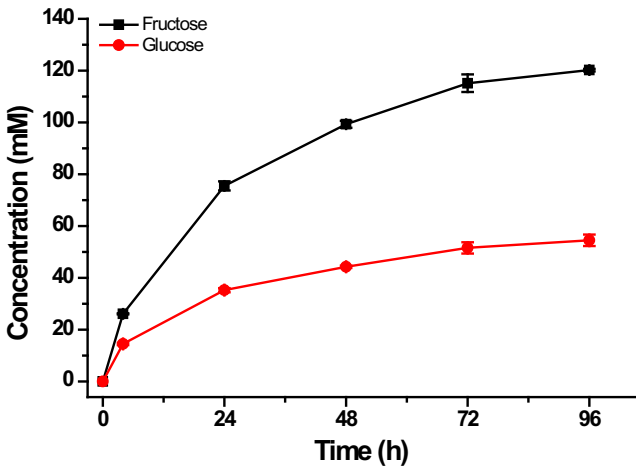

Fig. 6 Biosynthesis of fructose from 50 g/L maltodextrin by the in vitro synthetic enzymatic biosystem containing αGP, PGM, PGI, and Trd_1070. The reaction was performed at 70 °C under the condition of 50 g/L IA-treated maltodextrin (275 mM glucose equivalent), 100 mM HEPES buffer (pH 7.0), 10 mM $MgCl_2$, 50 mM phosphate, 0.30 U/mL αGP-containing cells, 0.30 U/mL PGM-containing cells, 1.20 U/mL PGI-containing cells, and 0.20 U/mL Trd_1070-containing cells

Discussion

Currently, fructose is mainly produced by the reversible isomerization of glucose which is carried out in aqueous phase by using glucose isomerase (GI, EC 5.3.1.5), resulting in the low product yield of fructose because of the thermodynamic equilibrium of GI (Li et al. 2017). In addition, inactivation of GI at higher temperatures, the narrow pH operation window, inhibitory effect by Ca^{2+}, and the requirement of Co^{2+} by GI are the major drawbacks of this process (Li et al. 2017). Exploration for more efficient routes to produce fructose is therefore of great interest. A thermodynamically favorable metabolic pathway containing alpha-glucan phosphorylase, phosphoglucomutase, phosphoglucose isomerase, and fructose-6-phosphatase was proposed to produce fructose from maltodextrin (Moradian and Benner 1992). The final exergonic step catalyzed by fructose-6-phosphatase pulls reaction intermediates to fructose thoroughly. However, the phosphatase that selectively dephosphorylates F6P in the final exergonic step has not been found yet (Moradian and Benner 1992). In our study, the catalytic efficiency of Trd_1070 for F6P was 49-fold higher than that for G6P and 296-fold higher than that for G1P; Trd_1070 seemed to be the appropriate phosphatase for F6P dephosphorylation (Table 3). Thus, Trd_1070 was recruited into this reported four-enzyme biosystem to produce fructose from maltodextrin (Fig. 5a). As shown in Fig. 6, 21.6 g/L fructose was produced from 50 g/L IA-treated maltodextrin. Due to the side reaction of Trd_1070 toward G6P, glucose was produced as a byproduct, and the ratio of fructose to glucose was approximate 2:1 (Fig. 6). Compared with the traditional GI-mediated fructose production method that usually gives a mixture of fructose and glucose at a ratio of approximately 1:1, the production cost of pure fructose by our in vitro synthetic biosystem would be lower.

In order to obtain the high fructose yield from maltodextrin, two main aspects should be taken into account. One is the utilization of remaining maltose and maltotriose because αGP cannot utilize these two compounds. The other is obtaining a highly specific F6P phosphatase, which shows little activity on G6P and G1P. To improve the utilization of maltodextrin, 4-glucanotransferase (4GT, EC 2.4.1.25), which transfers the anhydroglucose unit of maltose/maltotriose to another maltodextrin to obtain a longer maltodextrin chain for αGP utilization, can be added into the reaction mixture (You et al. 2017). For obtaining a highly specific F6P phosphatase, the mining of new specific phosphatase or the engineering of the current Trd_1070 by directed

evolution using high-throughput screening method (Senn and Wolosiuk 2005) can be performed in the future. In addition, fructose and glucose can lead to Maillard reaction, which may deactivate the enzymes and lead to incomplete utilization of substrates. For efficient utilization of maltodextrin, Maillard reactions can be alleviated by decreasing pH, adding antioxidants, or acetylating amino groups (Meng et al. 2018). In a word, deep investigation of this in vitro enzymatic biosystem for fructose production is required in the future to reduce the product cost in industrial scale, such as optimization of the process, reaction scale-up, and product separation.

For the in vitro enzymatic biosystems, a design principle is that the last step should be irreversible to maximize the product yield (You and Zhang 2017). As an enzyme that catalyzes irreversible exergonic reactions, phosphatase meets this design principle exactly, and can push the overall reaction toward completeness, resulting in a theoretical 100% conversion. For example, inositol was produced from starch or cellulose with a yield of more than 90% by in vitro synthetic enzymatic biosystems with the assist of inositol monophosphate (Meng et al. 2018; You et al. 2017). Therefore, after finding new phosphatases with high specificity on certain sugar phosphates, this in vitro synthetic biosystem can be used as a universal and efficient biomanufacturing platform for the production of many valuable monosaccharides such as tagatose, allulose, and mannose.

In this work, we performed the enzymatic characterization of a thermostable sugar phosphatase Trd_1070 from *T. roseum*. This enzyme exhibited much higher activity of dephosphorylation toward F6P than G6P and G1P; thus, a four-enzyme in vitro synthetic enzymatic biosystem including Trd_1070 was constructed to produce fructose from maltodextrin, providing a cost-efficient route for the production of fructose. After finding new phosphatases with highly specificity on specific sugar phosphates, the phosphatase-included in vitro synthetic enzymatic biosystem will become a universal and efficient biomanufacturing platform for the production of value-added monosaccharides, such as low-calorie rare sugars, from low-cost biomass.

Funding information This work was supported by the Key Research Program of the Chinese Academy of Sciences (Grant No. ZDRW-ZS-2016-3), the National Natural Science Foundation of China (Grant No. 31600635 and 21778073), and the 1000-youth talent program of China.

Compliance with ethical standards

Conflict of interest The authors declare that they have no competing interest.

Ethical statement This article does not contain any studies with human participants or animals performed by any of the authors.

References

Allen KN, Dunaway-Mariano D (2004) Phosphoryl group transfer: evolution of a catalytic scaffold. Trends Biochem Sci 29(9):495–503. https://doi.org/10.1016/j.tibs.2004.07.008

Aravind L, Galperin MY, Koonin EV (1998) The catalytic domain of the P-type ATPase has the haloacid dehalogenase fold. Trends Biochem Sci 23(4):127–129. https://doi.org/10.1016/S0968-0004(98)01189-X

Burroughs AM, Allen KN, Dunaway-Mariano D, Aravind L (2006) Evolutionary genomics of the HAD superfamily: understanding the structural adaptations and catalytic diversity in a superfamily of phosphoesterases and allied enzymes. J Mol Biol 361(5):1003–1034. https://doi.org/10.1016/j.jmb.2006.06.049

Collet JF, Stroobant V, Pirard M, Delpierre G, Van Schaftingen E (1998a) A new class of phosphotransferases phosphorylated on an aspartate residue in an amino-terminal DXDX(T/V) motif. J Biol Chem 273(23):14107–14112. https://doi.org/10.1074/jbc.273.23.14107

Collet JF, Van Schaftingen E, Stroobant V (1998b) A new family of phosphotransferases related to P-type ATPases. Trends Biochem Sci 23(8):284–284. https://doi.org/10.1016/S0968-0004(98)01252-3

Dong H, Secundo F, Xue C, Mao X (2017) Whole-cell biocatalytic synthesis of cinnamyl acetate with a novel esterase from the DNA library of *Acinetobacter hemolyticus*. J Agric Food Chem 65(10):2120–2128. https://doi.org/10.1021/acs.jafc.6b05799

Guo Z, Wang F, Shen T, Huang J, Wang Y, Ji C (2014) Crystal structure of thermostable p-nitrophenylphosphatase from *Bacillus Stearothermophilus* (Bs-TpNPPase). Protein Pept Lett 21(5):483–489. https://doi.org/10.2174/0929866520666131119200255

Huang H, Pandya C, Liu C, Al-Obaidi NF, Wang M, Zheng L, Toews Keating S, Aono M, Love JD, Evans B, Seidel RD, Hillerich BS, Garforth SJ, Almo SC, Mariano PS, Dunaway-Mariano D, Allen KN, Farelli JD (2015) Panoramic view of a superfamily of phosphatases through substrate profiling. Proc Natl Acad Sci U S A 112(16):E1974–E1983. https://doi.org/10.1073/pnas.1423570112

Kim CS, Seo JH, Kang DG, Cha HJ (2014) Engineered whole-cell biocatalyst-based detoxification and detection of neurotoxic organophosphate compounds. Biotechnol Adv 32(3):652–662. https://doi.org/10.1016/j.biotechadv.2014.04.010

Kuznetsova E, Proudfoot M, Gonzalez CF, Brown G, Omelchenko MV, Borozan I, Carmel L, Wolf YI, Mori H, Savchenko AV, Arrowsmith CH, Koonin EV, Edwards AM, Yakunin AF (2006) Genome-wide analysis of substrate specificities of the *Escherichia coli* haloacid dehalogenase-like phosphatase family. J Biol Chem 281(47):36149–36161. https://doi.org/10.1074/jbc.M605449200

Kuznetsova E, Nocek B, Brown G, Makarova KS, Flick R, Wolf YI, Khusnutdinova A, Evdokimova E, Jin K, Tan K, Hanson AD, Hasnain G, Zallot R, de Crecy-Lagard V, Babu M, Savchenko A, Joachimiak A, Edwards AM, Koonin EV, Yakunin AF (2015) Functional diversity of haloacid dehalogenase superfamily phosphatases from *Saccharomyces cerevisiae*: biochemical, structural, and evolutionary insights. J Biol Chem 290(30):18678–18698. https://doi.org/10.1074/jbc.M115.657916

Lahiri SD, Zhang GF, Dai JY, Dunaway-Mariano D, Allen KN (2004) Analysis of the substrate specificity loop of the HAD superfamily cap domain. Biochemistry 43(10):2812–2820. https://doi.org/10.1021/bi0356810

Larrouy-Maumus G, Biswas T, Hunt DM, Kelly G, Tsodikov OV, de Carvalho LPS (2013) Discovery of a glycerol 3-phosphate phosphatase reveals glycerophospholipid polar head recycling in *Mycobacterium tuberculosis*. Proc Natl Acad Sci U S A 110(28):11320–11325. https://doi.org/10.1073/pnas.1221597110

Lee SW, Oh MK (2016) Improved production of N-acetylglucosamine in *Saccharomyces cerevisiae* by reducing glycolytic flux. Biotechnol Bioeng 113(11):2524–2528. https://doi.org/10.1002/bit.26014

Li H, Yang S, Saravanamurugan S, Riisager A (2017) Glucose isomerization by enzymes and chemo-catalysts: status and current advances. ACS Catal 7(4):3010–3029. https://doi.org/10.1021/acscatal.6b03625

Lu Z, Dunaway-Mariano D, Allen KN (2008) The catalytic scaffold of the haloalkanoic acid dehalogenase enzyme superfamily acts as a mold for the trigonal bipyramidal transition state. Proc Natl Acad Sci U S A 105(15):5687–5692. https://doi.org/10.1073/pnas.0710800105

Meng D, Wei X, Zhang Y-HPJ, Zhu Z, You C, Ma Y (2018) Stoichiometric conversion of cellulosic biomass by in vitro synthetic enzymatic biosystems for biomanufacturing. ACS Catal 8:9550–9559. https://doi.org/10.1021/acscatal.8b02473

Mitchell AL, Attwood TK, Babbitt PC, Blum M, Bork P, Bridge A, Brown SD, Chang HY, El-Gebali S, Fraser MI, Gough J, Haft DR, Huang H, Letunic I, Lopez R, Luciani A, Madeira F, Marchler-Bauer A, Mi H, Natale DA, Necci M, Nuka G, Orengo C, Pandurangan AP, Paysan-Lafosse T, Pesseat S, Potter SC, Qureshi MA, Rawlings ND, Redaschi N, Richardson LJ, Rivoire C, Salazar GA, Sangrador-Vegas A, Sigrist CJA, Sillitoe I, Sutton GG, Thanki N, Thomas PD, Tosatto SCE, Yong SY, Finn RD (2019) InterPro in 2019: improving coverage, classification and access to protein sequence annotations. Nucleic Acids Res 47(D1):D351–D360. https://doi.org/10.1093/nar/gky1100

Moradian A, Benner SA (1992) A biomimetic biotechnological process for converting starch to fructose: thermodynamic and evolutionary considerations in applied enzymology. J Am Chem Soc 114(18):6980–6987. https://doi.org/10.1021/ja00044a005

Morais MC, Zhang WH, Baker AS, Zhang GF, Dunaway-Mariano D, Allen KN (2000) The crystal structure of *Bacillus cereus* phosphonoacetaldehyde hydrolase: insight into catalysis of phosphorus bond cleavage and catalytic diversification within the HAD enzyme superfamily. Biochemistry 39(34):10385–10396. https://doi.org/10.1021/bi001171j

Motosugi K, Esaki N, Soda K (1982) Purification and properties of a new enzyme, DL-2-haloacid dehalogenase, from *Pseudomonas* sp. J Bacteriol 150(2):522–527

Ninh PH, Honda K, Yokohigashi Y, Okano K, Omasa T, Ohtake H (2013) Development of a continuous bioconversion system using a thermophilic whole-cell biocatalyst. Appl Environ Microbiol 79(6):1996–2001. https://doi.org/10.1128/AEM.03752-12

Rangarajan ES, Proteau A, Wagner J, Hung MN, Matte A, Cygler M (2006) Structural snapshots of *Escherichia coli* histidinol phosphate phosphatase along the reaction pathway. J Biol Chem 281(49):37930–37941. https://doi.org/10.1074/jbc.M604916200

Riesenberg D, Schulz V, Knorre WA, Pohl HD, Korz D, Sanders EA, Ross A, Deckwer WD (1991) High cell-density cultivation of *Escherichia coli* at controlled specific growth-rate. J Biotechnol 20(1):17–28. https://doi.org/10.1016/0168-1656(91)90032-Q

Rinaldo-Matthis A, Rampazzo C, Reichard P, Bianchi V, Nordlund P (2002) Crystal structure of a human mitochondrial deoxyribonucleotidase. Nat Struct Biol 9(10):779–787. https://doi.org/10.1038/nsb846

Saheki S, Takeda A, Shimazu T (1985) Assay of inorganic phosphate in the mild pH range, suitable for measurement of glycogen phosphorylase activity. Anal biochem 148(2):277–281

Senn AM, Wolosiuk RA (2005) A high-throughput screening for phosphatases using specific substrates. Anal Biochem 339(1):150–156. https://doi.org/10.1016/j.ab.2004.12.021

Shen T, Guo Z, Ji C (2014) Structure of a His170Tyr mutant of thermostable pNPPase from *Geobacillus stearothermophilus*. Acta Crystallogr Sect F Struct Biol Commn 70(6):697–702. https://doi.org/10.1107/s2053230x14007341

Tamura K, Stecher G, Peterson D, Filipski A, Kumar S (2013) MEGA6: molecular evolutionary genetics analysis version 6.0. Mol Biol Evol 30(12):2725–2729. https://doi.org/10.1093/molbev/mst197

Tremblay LW, Dunaway-Mariano D, Allen KN (2006) Structure and activity analyses of *Escherichia coli* K-12 NagD provide insight into the evolution of biochemical function in the haloalkanoic acid dehalogenase superfamily. Biochemistry 45(4):1183–1193. https://doi.org/10.1021/bi051842j

Wang WR, Kim R, Jancarik J, Yokota H, Kim SH (2001) Crystal structure of phosphoserine phosphatase from *Methanococcus jannaschii*, a hyperthermophile, at 1.8 angstrom resolution. Structure 9(1):65–71. https://doi.org/10.1016/S0969-2126(00)00558-X

Wang W, Liu M, You C, Li Z, Zhang Y-HP (2017) ATP-free biosynthesis of a high-energy phosphate metabolite fructose 1,6-diphosphate by in vitro metabolic engineering. Metab Eng 42:168–174. https://doi.org/10.1016/j.ymben.2017.06.006

You C, Zhang Y-HP (2013) Self-assembly of synthetic metabolons through synthetic protein scaffolds: one-step purification, co-immobilization, and substrate channeling. ACS Synth Biol 2(2):102–110. https://doi.org/10.1021/sb300068g

You C, Zhang Y-HP (2017) Biomanufacturing by in vitro biosystems containing complex enzyme mixtures. Process Biochem 52:106–114. https://doi.org/10.1016/j.procbio.2016.09.025

You C, Shi T, Li Y, Han P, Zhou X, Zhang Y-HP (2017) An in vitro synthetic biology platform for the industrial biomanufacturing of myo-inositol from starch. Biotechnol Bioeng 114(8):1855–1864. https://doi.org/10.1002/bit.26314

Zhang G, Morais MC, Dai J, Zhang W, Dunaway-Mariano D, Allen KN (2004) Investigation of metal ion binding in phosphonoacetaldehyde hydrolase identifies sequence markers for metal-activated enzymes of the HAD enzyme superfamily. Biochemistry 43(17):4990–4997. https://doi.org/10.1021/bi036309n

Zhou R, Cheng L, Wayne R (2003) Purification and characterization of sorbitol-6-phosphate phosphatase from apple leaves. Plant Sci 165(1):227–232. https://doi.org/10.1016/s0168-9452(03)00166-3

Zhou W, You C, Ma H, Ma Y, Zhang Y-HP (2016) One-pot biosynthesis of high-concentration alpha-glucose 1-phosphate from starch by sequential addition of three hyperthermophilic enzymes. J Agric Food Chem 64(8):1777–1783. https://doi.org/10.1021/acs.jafc.5b05648